Acta Oceanol. Sin., 2018, Vol. 37, No. 3, P. 103–110
DOI: 10.1007/s13131-018-1203-7
http://www.hyxb.org.cn
E-mail: hyxbe@263.net

Estimating significant wave height from SAR imagery based on an SVM regression model

GAO Dong[1, 2], LIU Yongxin[1], MENG Junmin[2], JIA Yongjun[3], FAN Chenqing[2]*

[1] College of Electronic and Information Engineering, Inner Mongolia University, Hohhot 010020, China

[2] The First Institute of Oceanography, State Oceanic Administration, Qingdao 266061, China

[3] National Satellite Ocean Application Service, State Oceanic Administration, Beijing 100081, China

Received 17 January 2017; accepted 31 May 2017

Abstract

A new method for estimating significant wave height (SWH) from advanced synthetic aperture radar (ASAR) wave mode data based on a support vector machine (SVM) regression model is presented. The model is established based on a nonlinear relationship between σ^0, the variance of the normalized SAR image, SAR image spectrum spectral decomposition parameters and ocean wave SWH. The feature parameters of the SAR images are the input parameters of the SVM regression model, and the SWH provided by the European Centre for Medium-range Weather Forecasts (ECMWF) is the output parameter. On the basis of ASAR matching data set, a particle swarm optimization (PSO) algorithm is used to optimize the input kernel parameters of the SVM regression model and to establish the SVM model. The SWH estimation results yielded by this model are compared with the ECMWF reanalysis data and the buoy data. The RMSE values of the SWH are 0.34 and 0.48 m, and the correlation coefficient is 0.94 and 0.81, respectively. The results show that the SVM regression model is an effective method for estimating the SWH from the SAR data. The advantage of this model is that SAR data may serve as an independent data source for retrieving the SWH, which can avoid the complicated solution process associated with wave spectra.

Key words: advanced synthetic aperture radar wave mode, support vector machine, significant wave height

Citation: Gao Dong, Liu Yongxin, Meng Junmin, Jia Yongjun, Fan Chenqing. 2018. Estimating significant wave height from SAR imagery based on an SVM regression model. Acta Oceanologica Sinica, 37(3): 103–110, doi: 10.1007/s13131-018-1203-7

1 Introduction

Ocean wave is an important research topic in physical oceanography, and a significant wave height (SWH) is one of the most important parameters of an ocean wave observation. The classical SWH inversion methods are an algorithm developed by the Max Planck Institute (MPI), a partition rescale and shift algorithm (PARSA), and a semiparametric retrieval algorithm (SPRA). The SWH retrieved by the MPI is based on the nonlinear mapping relation between the wave spectrum and the image spectrum of a SAR image. Although good SWH results can be obtained, MPI must run an ocean wave numerical model (such as WAM) to obtain a first-guess spectrum (Hasselmann and Hasselmann, 1991; Hasselmann et al., 1996). The PARSA method is an improvement and extension of the MPI method. Compared with buoy measurements, the PARSA method yields better inversion results, but it requires the multi-view cross-spectrum of a SAR image as the input for inversion. The SPRA algorithm requires external synchronized wind field information, and the wind vector parameter is used as an input to obtain ocean wave spectra (Mastenbroek and de Valk, 2000). In analyzing the MPI and SPRA algorithms for the wave spectrum inversion, Sun and Guan (2006) outlined the advantages and disadvantages of the two. An improved parameterized preliminary guessing spectrum model was used as an input of the inversion, and the SAR image spectrum was divided into wind and wave spectra to retrieve SWH.

At present, an empirical CWAVE model (Schulz-Stellenfleth et al., 2007) and a CWAVE_ENV model (Li et al., 2011) are mainly applied to retrieving the SWH. Both models are second-order multiple regression models. The main difference between them is the SAR data used to retrieve the SWH. To avoid the problem of having too many unknown parameters in a polynomial regression model, the researchers put forward a new method based on a support vector machine (SVM) regression model. The SVM is a new machine learning algorithm generated within the framework of a computational learning theory. The SVM is mainly used for data classification, but a version of the SVM for regression was proposed by Vapnik (1998), which has made it possible to apply the SVM as a regression estimation model (Elbisy, 2015; Wang and Bai, 2014; Xu et al., 2016). Compared with the classical ocean wave spectrum inversion methods, the SVM regression model does not need additional data as inputs; the SAR data can be used as an independent data source for SWH extraction. Furthermore, compared with the second-order multiple regression models, it is able to solve the problem of poor learning, over learning and poor generalization. The SVM-based SWH extraction method proposed in this paper provides a new choice for estimating the SWH from the SAR imagery.

Foundation item: The National Key Research and Development Program of China under contract Nos 2016YFA0600102 and 2016YFC1401007; the National Natural Science Youth Foundation of China under contract No.61501130; the Natural Science Foundation of China under contract No. 41406207.

*Corresponding author, E-mail: fanchenqing@fio.org.cn

2 Data

2.1 *SAR data*

The data used in this study are wave mode global ocean data provided by an ASAR sensor mounted on the ENVISAT satellite. The SWH retrieval model is established by using 17 200 scenes of ASAR wave mode data covering an area of 5 km×10 km, which match the ECMWF reanalysis data obtained in January 2011. The 42 774 ASAR wave mode images match the reanalysis data obtained in April and May 2011 and are used to validate the SVM model independently. The parameters of the ASAR wave mode data are shown in Table 1.

Table 1. Parameters of SLC images of ENVISAT ASAR wave mode

Parameter	ENVISAT ASAR
Band	C (5.3 GHz)
Polarization	HH or VV
Incidence angle θ/(°)	14.1–42.3
Azimuth spacing/m	4.0
Range spacing/m	7.0
Swath width/m	5 000

2.2 *ECMWF data*

An important feature of the ECMWF reanalysis data is the assimilation of altimeter data. The SWH data assimilated by the global atmospheric reanalysis (ERA-interim) data have been updated since 1979 and provide high accuracy in the ocean wave observation. In this study, the SWH data provided by the ERA-Interim were chosen to serve as the output of SVM regression modeling. The spatial resolution was 0.125°×0.125°, and the temporal resolution was 6 h. The data were acquired in January, April and May 2011.

2.3 *Buoy data*

Buoy data is one of the important means of measuring the SWH. Most buoys are distributed in coastal waters and provide reliable data for validating SAR inversion results. In this study, we used 96 buoys to match the ASAR wave mode data. Finally, we found only 12 buoy stations that could match our SAR data. Table 2 shows location information for the 12 buoys that provided the *in situ* validation dataset. Most of the buoys are located in the Gulf of Mexico. The temporal resolution of the buoy data is 1 h. Table 2 and Fig. 1 show the buoy parameters.

The quality control of the SWH measured by buoys is a key step in temporal and spatial matching between the buoy data and the SAR data. In this study, the buoy data were used to validate our SVM regression model, with the SWH ranging between 0 and 25 m. The temporal resolution of the buoy data is 1 h. In areas with high sea-level fluctuations, the difference in the SWH from moment to moment is no more than 10 m (Park et al., 2013). Therefore, the peak detection method was applied to further filtering the buoy data. The buoy data obtained after processing were considered to be independent data for validating the SVM regression model.

3 Model description

In this study, the regression model for retrieving the SWH was established by the SVM. On the basis of a structured risk minimization theory and a convex optimization theory, this method can find a compromise between the accuracy of a given data approximation and the complexity of the corresponding function. Finally, the SVM model can obtain good generalizability. Twenty-two feature parameters were extracted from the spatial and frequency domains of homogeneous SAR images as the SVM model input; the SWH of the ERA-Interim data matched with the SAR images was the output of the SVM model. The optimal radial basis function (RBF) kernel parameters were obtained through particle swarm optimization (PSO), and the SVM model was established. Figure 2 shows the overall flow chart of the SVM modeling process.

3.1 *SAR image homogeneity test*

Depending on the process used to extract feature parameters from SAR images, the quality of the SAR images can affect the extraction of the SWH. For example, atmospheric phenomena such as boundary layer rolls (Alpers and Brümmer, 1994), atmospheric fronts, rain cells (Melsheimer et al., 1998), and the surface slicks of anthropogenic or biological origin (Gade et al., 1998) will affect the imaging process of the ENVISAT satellite, which makes intensity images appear inhomogeneous. These images should be removed during the establishment of the SVM model. Therefore, it is necessary to test the homogeneity of the ASAR wave mode images and then match the results with ECMWF reanalysis data. According to a standard spectral estimation theory, spectral density Φ_k estimated from the periodogram of homogeneous ASAR wave mode images is negative exponentially distributed (Schulz-Stellenfleth and Lehner, 2004). The relationship between the variance of the spectral density $\sigma^2(\Phi_k)$ and the mean value $\overline{\Phi_k^2}$ is

$$\frac{\sigma^2(\Phi_k)}{\overline{\Phi_k^2}} \approx 1. \tag{1}$$

To reduce the deviation in ASAR wave mode images, each subimage can be divided into 256×512 subimage blocks. The operation described by Eq. (2) is performed for each subimage block, and the average is taken as the threshold for testing the SAR image homogeneity. Equation (2) is used for verification, where N is the number of subimage blocks:

$$\hat{\xi} = \frac{1}{N}\sum_{k=1}^{N} \frac{\sigma^2(\hat{\Phi}_k)}{\overline{\hat{\Phi}_k^2}}. \tag{2}$$

Table 2. Parameters of buoys

Buoy ID	North latitude	West longitude	Depth/m	Buoy ID	North latitude	West longitude	Depth/m
41040	14°30′	53°01′	4 900.0	41041	14°19′	46°04′	3 485.0
42001	25°53′	89°39′	3 365.0	42002	26°05′	93°45′	3 125.0
42019	27°54′	95°21′	83.0	42020	26°58′	96°41′	79.9
42035	29°13′	94°24′	15.0	42040	29°12′	88°12′	37.0
42055	22°12′	94°00′	3 595.0	46083	58°17′	139°59′	136.0
46082	59°10′	143°23′	296.0	46085	55°52′	142°29′	3 736.0

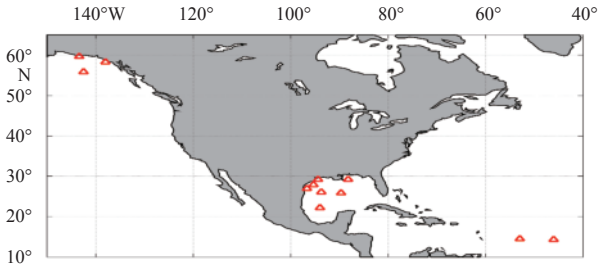

Fig. 1. Location of collocated buoys used for SVM model validation.

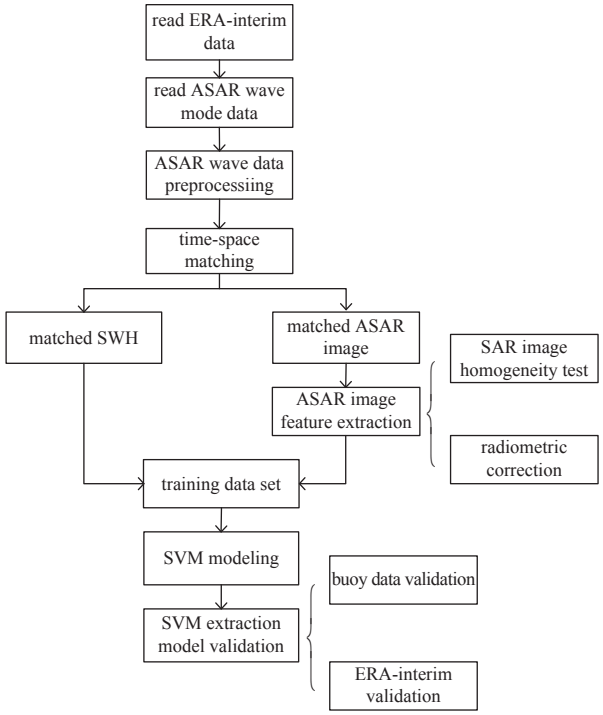

Fig. 2. SVM modeling process.

On the basis of the statistical analysis of ASAR wave mode images, a threshold of 1.05 is used as the criterion to test the SAR images (Schulz-Stellenfleth and Lehner, 2004). Figure 3 shows a diagram of the ASAR image block division process.

The spatial and temporal matching windows are 100 km and 2 h, respectively. The feature parameters of homogeneous the SAR imagery were extracted for modeling and to validate the SVM regression model.

3.2 *SAR image feature extraction*

3.2.1 *Spatial domain parameters*

SAR image feature parameters represent an important index for reflecting information about the sea states. Whether the extraction of the image feature parameters is feasible will directly affect the accuracy with which the SWH is retrieved using an SVM regression model. The SAR imagery statistical analysis shows that the image variance (σ_i^2) and the average backscatter coefficient σ_0 of images show a quasi-approximate linear relationship with SWH. Therefore, the image variance and the average backscatter coefficient (σ_0) were selected as the image feature parameters required to establish the SVM regression model.

During SAR imaging, the uncertainty in the transmit power, receive gain, antenna pattern and other parameters of the radar system cannot accurately reflect echo characteristics. Therefore, it is necessary to submit the SAR images to radiometric calibration (Singh et al., 2007). The average backscatter coefficient and variance of the images after a radiation correction can thus be obtained as follows:

$$\sigma_0 = \frac{\langle I \rangle}{K} \frac{1}{G^2(\theta_d)} \left(\frac{R_d}{R_{ref}} \right)^3 \sin(\alpha_d), \tag{3}$$

$$\sigma_i^2 = \left[\mathrm{std}\left(\frac{I - \langle I \rangle}{\langle I \rangle} \right) \right]^2, \tag{4}$$

where K is the absolute calibration constant; $\langle I \rangle$ is the average value of the wave mode intensity image; and σ_0 is the mean value of the backscattering coefficient after image radiometric calibration. R_d is the slant range; R_{ref} is the reference slant range; and α_d is the angle of incidence. These parameters can be obtained by reading the WVI data file. $G^2(\theta_d)$ is the two-way mode gain value obtained through the radiometric calibration of auxiliary files.

3.2.2 *Frequency domain parameters*

Obtaining structural feature information from the frequency domain is a common approach in the field of remote sensing. To further extract sea-state features from the SAR images, the 20 feature parameters of the SAR images in the frequency domain are selected as the inputs of the SVM model. First, the images are submitted to Fourier transformation. A series of orthogonal functions are then used to decompose the SAR images to extract the feature parameter information in the frequency domain. The orthogonal function is composed of Gegenbauer polynomials and harmonic functions (Li et al., 2011):

$$h_{ij}(\alpha_k, \alpha_\varphi) = \eta(k_x, k_y) \mathrm{G}_i(\alpha_k) f_j(\alpha_\varphi),\ 1 \leqslant i \leqslant 4,\ 1 \leqslant j \leqslant 5, \tag{5}$$

where

$$\mathrm{G}_{n_k}(\alpha_k) = \sqrt{\frac{n_k + 3/2}{(n_k+2)(n_k+1)}} C_{n_k}^{3/2} \sqrt{1-\alpha_k^2}, \tag{6}$$

$$f_{n_{\varphi-1}}(\alpha_\varphi) = \sqrt{\frac{2}{\pi}} \sin\left[(n_\varphi - 1)\alpha_\varphi \right], \tag{7}$$

$$f_{n_\varphi}(\alpha_\varphi) = \sqrt{\frac{2}{\pi}} \cos\left[(n_\varphi - 1)\alpha_\varphi \right], \tag{8}$$

where $h_{ij}(\alpha_k, \alpha_\varphi)$ is the orthonormal function composed of Gegenbauer polynomials $G_i(\alpha_k)$ and harmonic functions $f_j(\alpha_\varphi)$; and $\eta(k_x, k_y)$ is the weight function associated with a wavenumber in the respective range and azimuth in Domain A, which features an elliptical integration area; $\mathrm{G}_i(\alpha_k)$ is the general expression for Gegenberg polynomials; n_k=1, 2, 3, 4 in this study; $f_{n_{\varphi-1}}$ and f_{n_φ} correspond to the odd and even terms of the harmonic function, respectively. The process for extracting the image feature parameters can be expressed as follows:

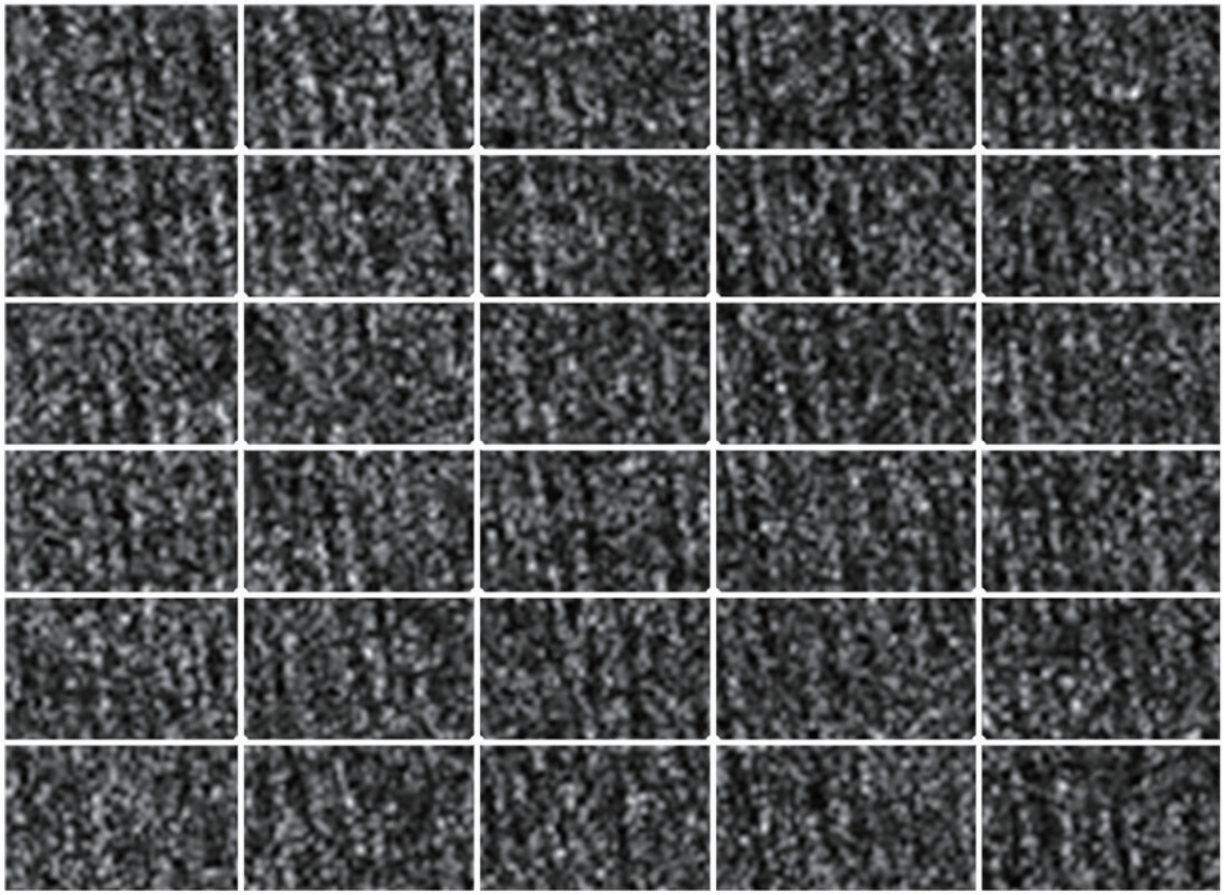

Fig. 3. ASAR wave mode image division.

$$x_i = \iint \overline{P}(k_x, k_y)\overline{h}_i(k_x, k_y)\mathrm{d}k_x\mathrm{d}k_y, 1 \leqslant i \leqslant n_\varphi n_k, \tag{9}$$

where $\overline{P}(k_x, k_y)$ is the normalized SAR image spectrum.

$$\overline{P} = P \cdot \left(\iint_A P(k_x, k_y)\mathrm{d}k_x\mathrm{d}k_y \right)^{-1}, \tag{10}$$

where P is the ASAR image power density spectrum. The remaining parameters are as determined by Schulz-Stellenfleth et al. (2006).

3.3 *SVM regression model*

3.3.1 *Support vector machine*

The SVM is a method developed from statistical theory and is based on the idea of the structured risk minimization. The algorithm proposed by Vapnik (1998) can minimize structural risk while minimizing the error of training samples. The SVM can be used for pattern classification and nonlinear regression prediction. For classification, the SVM attempts to classify samples by establishing a classifying hypersphere as a decision surface. In terms of SVM regression estimation, SVM modeling is based on the principle of classification by introducing an insensitive loss function $\varepsilon[f(x_i), y_i]$ (Suganyadevi et al., 2016; Fadel et al., 2016). Compared with polynomial regression models and neural networks, the SVM regression model has two advantages. On the one hand, the SVM regression model is not restricted by the dimensions of sample data and offers strong generalizability and high estimation accuracy. On the other hand, the basic objective of the SVM model is to map training samples from a low-dimensional space onto a high-dimensional space by mapping function $\phi(X)$. Finally, a nonlinear problem is transformed into a linear problem for fitting.

Homogeneous SAR images are used to establish a training data set $T = \{X_i, Y_i, i = 1, 2, ..., n\}$, where $X_i = \{1, x_{i,1}, x_{i,2}, ..., x_{i,22}\}$ is the feature vector extracted from one of the matching homogeneous SAR image samples; $Y \in R$ is the SWH value obtained by matching ECMWF; and n is the total number of samples. In the nonlinear regression problem, the regression model function is mapped onto the high-dimensional feature space F as follows:

$$f(X) = \overrightarrow{w}^{\mathrm{T}} \cdot \phi(X) + b, \tag{11}$$

where $\overrightarrow{w} = \{w_1, w_2, ..., w_k\}$ is the weight vector; $\phi(X)$ represents the high-dimensional feature space that has been nonlinearly mapped from the input space; b is a bias term; and $f(X)$ represents the SWH estimated by the model. In estimating the SVM regression model, $\overrightarrow{w}$ and b are unknown parameters. Therefore, the coefficients w and b are estimated by minimizing the following regularized risk function:

$$\min\ R(C) = \frac{1}{2}\|w\|^2 + C\frac{1}{l}\sum_{i=1}^{l} L\varepsilon\left[Y_i, f(X_i)\right], \tag{12}$$

$$L\varepsilon[Y_i, f(X_i)]=\begin{cases}|Y_i-f(X_i)|-\varepsilon, & |Y_i-f(X_i)|\geqslant\varepsilon,\\ 0, & |Y_i-f(X_i)|<\varepsilon,\end{cases} \tag{13}$$

where ε is a precision parameter representing the radius of the tube located around the regression function; $L\varepsilon$ is the insensitive loss function; C is a penalty constant used to seek a compromise between model generalization ability and training error. $\frac{1}{2}\|w\|^2$ determines the size of the hyperplane function interval, the smaller the value of this factor is, the larger the interval becomes. To reduce the error of the model, the slack variables ξ and ξ^* are introduced:

$$\min L(w, \xi_i, \xi_i^*)=\frac{1}{2}\|w\|^2+C\sum_{i=1}^{l}(\xi_i+\xi_i^*), \quad C>0, \tag{14}$$

subject to

$$\left.\begin{aligned}&Y_i-w^{\mathrm{T}}\cdot\phi(X_i)-b\leqslant\varepsilon+\xi_i, \ \xi_i>0\\ &w^{\mathrm{T}}\cdot\phi(X_i)+b-Y_i\leqslant\varepsilon+\xi_i^*, \ \xi_i^*>0\end{aligned}\right\}. \tag{15}$$

To solve the above-mentioned objective function problem, the Lagrangian form is constructed based on the constraint condition as follows:

$$\begin{aligned}L=&\frac{1}{2}\|w\|^2+C\sum_{i=1}^{l}(\xi_i+\xi_i^*)-\sum_{i=1}^{l}(\eta_i\xi_i+\eta_i^*\xi_i^*)-\\ &\sum_{i=1}^{l}\alpha_i(\varepsilon+\xi_i-Y_i+w^{\mathrm{T}}\cdot\phi(X_i)+b)-\\ &\sum_{i=1}^{l}\alpha_i^*(\varepsilon+\xi_i^*+Y_i-w^{\mathrm{T}}\cdot\phi(X_i)-b),\end{aligned} \tag{16}$$

where $\alpha_i>0$; $\alpha_i^*>0$; η_i and $\eta_i^*>0$. The following process is used to find the saddle point using the partial derivatives of L with respect to each Lagrangian multiplier for minimizing the function:

$$\frac{\partial L}{\partial b}=\sum_{i=1}^{l}(\alpha_i-\alpha_i^*)=0, \tag{17}$$

$$\frac{\partial L}{\partial w}=w-\sum_{i=1}^{l}(\alpha_i-\alpha_i^*)\phi(X_i)=0, \tag{18}$$

$$\frac{\partial L}{\partial \xi_i}=C-\alpha_i-\eta_i=0, \tag{19}$$

$$\frac{\partial L}{\partial \xi_i^*}=C-\alpha_i^*-\eta_i^*=0. \tag{20}$$

The optimization problem with inequality constraints can be transformed into the following dual optimization problem by substituting Eqs (17), (18), (19) and (20) into Eq. (16):

$$\begin{aligned}\max_{\alpha_i,\,\alpha_i^*}L(\alpha, \alpha^*)=&-\frac{1}{2}\sum_{i,j=1}^{l}(\alpha_i-\alpha_i^*)(\alpha_j-\alpha_j^*)K(X_i, X_j)-\\ &\varepsilon\sum_{i=1}^{l}(\alpha_i-\alpha_i^*)+\sum_{i=1}^{l}Y_i(\alpha_i+\alpha_i^*),\end{aligned} \tag{21}$$

subject to

$$\sum_{i=1}^{l}(\alpha_i-\alpha_i^*)=0, \ \alpha_i, \alpha_i^*\in[0, C], \tag{22}$$

where $K(X_i, X_j)=\phi(X_i)^{\mathrm{T}}\phi(X_j)$. Equation (11) can be written as follows:

$$f(x)=\sum_{i=1}^{l}(\alpha_i-\alpha_i^*)K(X_i, X)+b. \tag{23}$$

3.3.2 *SVM regression model parameters*

The estimation performance of the SVM regression model depends mainly on the kernel function and kernel parameters involved in model selection. Selecting a bad kernel function and corresponding kernel parameter will make the SVM incorrectly classified or estimated (Fadel et al., 2016). At present, the kernel functions include a linear kernel function, a polynomial kernel function, a sigmoidal kernel function and an RBF kernel function. Because a regression model for nonlinear problems was established in this study, an RBF was selected as the kernel function to establish the SVM regression model. Compared with other kernel functions, an RBF kernel function can map the original feature space onto infinite dimensions and transform a nonlinear problem into a linear problem. The foregoing factors make it easy to establish a regression model. Moreover, the RBF kernel has the advantage of having fewer parameters, which reduces the complexity of establishing a model. The RBFs have a wide convergence domain and can be adapted to various sample situations. The RBF kernel function is the most extensively used kernel function in SVM modeling to date and can be expressed as follows:

$$K(\vec{X}, \vec{X}_c)=\exp(-\gamma\|\vec{X}-\vec{X}_c\|^2), \tag{24}$$

where γ is the kernel parameter of the RBF; $\vec{X}$ is the input sample feature vector; and $\vec{X}_c$ is the kernel function center vector. The results of Vapnik (1998) show that when the SVM regression model is established, the parameters of the RBF kernel function and penalty factor C have a strong effect on the SVM results; therefore, it is necessary to adopt a suitable method for optimizing the RBF kernel parameters. A PSO algorithm was first suggested by Kennedy and Eberhart (1995). The PSO is easy to implement, with high precision and fast convergence (Behravan et al., 2016; Nisha and Pillai, 2013). Compared with the genetic algorithm, the PSO reduces the complex processes of "crossover" and "mutation" and has been widely used in parameter optimization (Wang, 2014). In optimization, the initial population is 50, the number of iterations is 200, $C\in[0.1, 100]$ and $\gamma\in[0.001, 100]$. On the basis of the training set, the training error of each particle is obtained, and the global average error is calculated. The population is updated iteratively based on the premise of meeting the loop conditions. Finally, the corresponding parameters C and γ are obtained.

In this study, the following kernel parameters were obtained by the PSO algorithm: $\gamma=0.008$ and $C=15$. The model was trained according to the input SVM regression model parameters γ and C. In the following expression, the number of effective support vectors is l, the support vector coefficients are an

$l\times1$ vector $\vec{\alpha}-\vec{\alpha}^*$, the global error is b, the support vector $\vec{X}_c$ is an $l\times n$ matrix, and n is the number of training sample features:

$$f(X)=\sum_{i=1}^{l}(\alpha_i-\alpha_i^*)\exp(-\gamma\| X-X_{ic}\|^2)+b. \tag{25}$$

3.4 *SVM fitting test*

The SVM regression model was established by using the January 2011 global matching data set. For ASAR wave mode data and ECMWF reanalysis data matching, the temporal window was 2 h, the spatial window was 100 km, and the number of matched pairs was 17 200. The training dataset of the SVM model was then used to test the fitness of the SVM model. Figure 4a shows the comparison results, whereas Fig. 4b shows the SWH distribution histogram.

The SVM regression model fitting test shows that the RMSE is 0.33 m, the correlation coefficient is 0.95 and the bias is 0.02 m, respectively. Therefore, the SVM regression model can be used to extract the SWH from the SAR data.

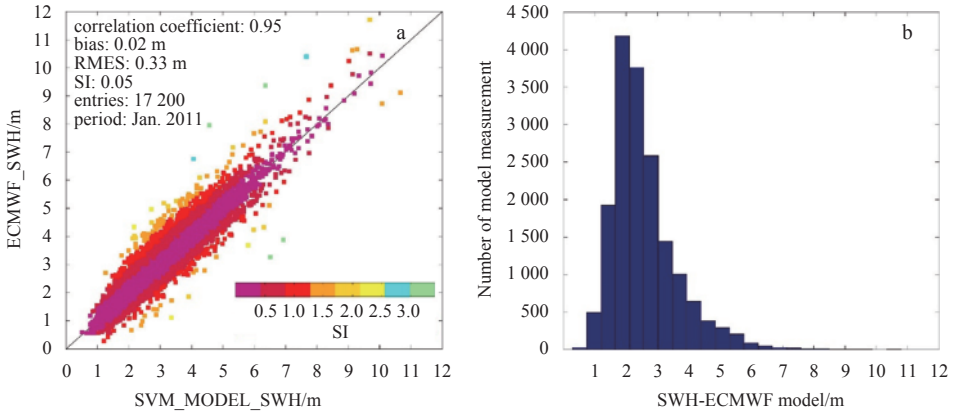

Fig. 4. Fitting test of SVM model. Comparison of SWH fitting test results (a) and SWH distribution (b).

4 Model validation

4.1 *Comparison with ECMWF data*

In this paper, the SAR data gathered in April 2011 and May 2011 and matched with the ECMWF reanalysis data were used to validate an SVM model. The matching temporal window was 2 h, the spatial window was 100 km, and 42 774 matching pairs were acquired from the global ocean data. Figure 5 shows the validation results obtained using the SVM model and the matched dataset, and the corresponding SWH histogram.

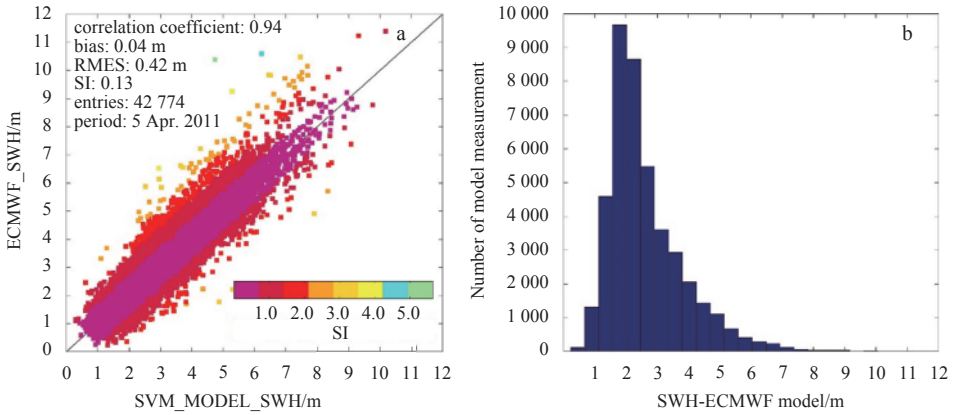

Fig. 5. Scatter plot of SWH derived by the SVM regression compared with ECMWF (a) and histogram showing ECMWF SWH distribution (b).

According to the distribution of different regions according to the color error band, the deviation in the SWH data between high- and low-sea conditions is less than 0.5 m. Thus, the SVM regression model is suitable for the SWH extraction under high- and low-sea conditions. In addition, the SWH deviation is large for certain SAR data, possibly because feature extraction from images was not precise. The SAR data may be contaminated by sea surface effects during imaging, which may result in a large deviation in the SVM model.

4.2 *Comparison with buoy data*

Buoy data distributed in the Gulf of Mexico were selected to validate the SWH retrieved by the SVM model. Fewer effective observational data matched the buoy data when the temporal window was set to 0.5 h. Using a 1 h temporal window for sea conditions produced no obvious changes. Therefore, the temporal window used to match SAR data with buoy data was set to 1 h and the spatial window was set to 200 km. A total of 2 553 scene data were matched. The SVM model results obtained using the

independent SAR data are shown in Fig. 6; Fig. 6a shows the SVM model estimation results compared with the buoy-measured results, and Fig. 6b shows the buoy-measured SWH histogram.

Figure 6a shows that the SWH results extracted by the SVM model are good. Compared with the matched buoy data, the RMSE is 0.48 m, the deviation is 9 cm and the scattering index (SI) is 0.24. The histogram buoy data distribution shown in Fig. 6b indicates that 82% of the SWH data fall between 0.8 and 3.0 m. The SVM model was applied to testing the SAR data. The RMSE was determined to be 0.36 m, the SI was 0.19, and the bias was 5 cm. In short, the validation results obtained using the buoy data show that the SVM model exhibits good performance for middle- and high-sea conditions.

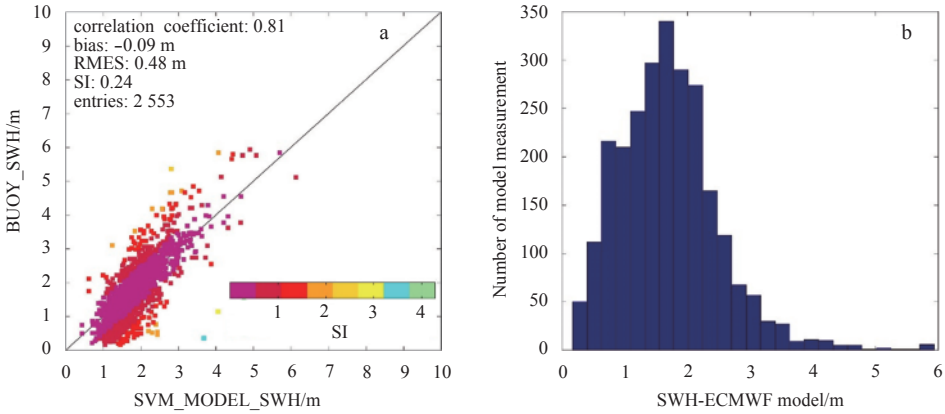

Fig. 6. Scatter plot of SWH derived by the SVM regression compared with buoy data (a) and buoy SWH distribution (b).

5 Conclusions

In this paper, the SWH retrieval model based on the SVM is established using an ASAR wave mode matching dataset. The SVM model shows good inversion results for high- and low-sea conditions. Twenty-two feature parameters were extracted as training samples from the spatial and frequency domains of the SAR images to fully reflect the quasi-linear relationship between the SAR images and the SWH. In the model, the feature parameters extracted from the SAR images were used as input, and the SWH obtained from the ECMWF was the output. An RBF was selected as the kernel function to establish the model. Validated by 2 553 ASAR wave data matched with buoy data and 42 774 ASAR data matched with ECMWF data, the SVM model was shown to extract the SWH data from the SAR data accurately. The RMSE values were 0.48 and 0.42 m, the deviations were 9 and 4 cm and the scattering index values were 0.24 and 0.13, respectively. In short, it is possible to retrieve the SWH from the SAR data as an independent data source based on the proposed SVM model. This method is an effective and feasible technology for extracting the SWH.

Acknowledgements

The authors thank the ESA for providing the ASAR data and the European Centre for Medium-range Weather Forecasts (ECMWF) for providing the reanalysis data (http://www.ecmwf.int/en/research/climate-reanalysis/browse-reanalysis-datasets). The authors also thank NDBC for providing the measured buoy data (http://www.ndbc.noaa.gov/).

References

Alpers W, Brümmer B. 1994. Atmospheric boundary layer rolls observed by the synthetic aperture radar aboard the ERS-1 satellite. Journal of Geophysical Research, 99(C6): 12613–12621

Behravan I, Dehghantanha O, Zahiri S H, et al. 2016. An optimal SVM with feature selection using multiobjective PSO. Journal of Optimization, 2016: 6305043

Elbisy M S. 2015. Support vector machine and regression analysis to predict the field hydraulic conductivity of sandy soil. KSCE Journal of Civil Engineering, 19(7): 2307–2316

Fadel S, Ghoniemy S, Abdallah M, et al. 2016. Investigating the effect of different kernel functions on the performance of SVM for recognizing Arabic characters. International Journal of Advanced Computer Science and Applications, 7(1): 446–450

Gade M, Alpers W, Hühnerfuss H, et al. 1998. Imaging of biogenic and anthropogenic ocean surface films by the multifrequency/multipolarization SIR-C/X-SAR. Journal of Geophysical Research, 103(C9): 18851–18866

Hasselmann S, Brüning C, Hasselmann K, et al. 1996. An improved algorithm for the retrieval of ocean wave spectra from synthetic aperture radar image spectra. Journal of Geophysical Research, 101(C7): 16615–16629

Hasselmann K, Hasselmann S. 1991. On the nonlinear mapping of an ocean wave spectrum into a synthetic aperture radar image spectrum and its inversion. Journal of Geophysical Research, 96(C6): 10713–10729

Kennedy J, Eberhart R. 1995. Particle swarm optimization. In: Proceedings of IEEE International Conference on Neural Networks. Perth, WA: IEEE, 1942–1948

Li Xiaoming, Lehner S, Bruns T. 2011. Ocean wave integral parameter measurements using envisat ASAR wave mode data. IEEE Transactions on Geoscience and Remote Sensing, 49(1): 155–174

Mastenbroek C, de Valk C F. 2000. A semiparametric algorithm to retrieve ocean wave spectra from synthetic aperture radar. Journal of Geophysical Research, 105(C2): 3497–3516

Melsheimer C, Alpers W, Gade M. 1998. Investigation of multifrequency/multipolarization radar signatures of rain cells over the ocean using SIR-C/X-SAR data. Journal of Geophysical Research, 103(C9): 18867–18884

Nisha M G, Pillai G N. 2013. Nonlinear model predictive control with relevance vector regression and particle swarm optimization. Journal of Control Theory and Applications, 11(4): 563–569

Park K A, Woo H J, Lee E Y, et al. 2013. Validation of significant wave height from satellite altimeter in the seas around Korea and error characteristics. Korean Journal of Remote Sensing, 29(6): 631–644

Schulz-Stellenfleth J, König T, Lehner S. 2007. An empirical approach for the retrieval of integral ocean wave parameters from synthetic aperture radar data. Journal of Geophysical Research, 112(C3): doi: 10.1029/2006JC003970

Schulz-Stellenfleth J, König T, Lehner S. 2006. Retrieval of integral ocean wave parameters from SAR data using an empirical approach. In: Proceedings of SEASAR 2006. 1–6

Schulz-Stellenfleth J, Lehner S. 2004. Measurement of 2-D sea surface elevation fields using complex synthetic aperture radar data. IEEE Transactions on Geoscience and Remote Sensing, 42(6): 1149–1160

Singh G, Kumar V, Vekataraman G, et al. 2007. Snow porosity estimation using advanced synthetic aperture radar single look complex data analysis and its effects on backscattering coefficient. Journal of Applied Remote Sensing, 1(1): 013522

Suganyadevi M V, Babulal C K, Kalyani S. 2016. Assessment of voltage stability margin by comparing various support vector regression models. Soft Computing, 20(2): 807–818

Sun Jian, Guan Changlong. 2006. Parameterized first-guess spectrum method for retrieving directional spectrum of swell-dominated waves and huge waves from SAR images. Chinese Journal of Oceanology and Limnology, 24(1): 12–20

Vapnik V N. 1998. Statistical Learning Theory. New York: Wiley

Wang Cheng. 2014. Optimization of SVM method with RBF kernel. Applied Mechanics and Materials, 496-500: 2306–2310

Wang Long, Bai Yanping. 2014. Research on prediction of air quality index based on NARX and SVM. Applied Mechanics and Materials, 602-605: 3580–3584

Xu Qifa, Jiang Cuixia, He Yaoyao. 2016. An exponentially weighted quantile regression via SVM with application to estimating multiperiod VaR. Statistical Methods & Applications, 25(2): 285–320